Supplementary Information for:

Nitrogen and transition-metal codoped titania nanotube arrays for visible-light-sensitive photoelectrochemical water oxidation

Tomiko M. Suzuki*, Gaku Kitahara, Takeo Arai, Yoriko Matsuoka and Takeshi Morikawa
Toyota Central Research & Development Labs. Inc., Nagakute, Aichi 480-1192, Japan.
Email: tomiko@mosk.tytlabs.co.jp

Preparation of Ti- transition metal (Ti-TM) alloys:

Ti-TM alloys were fabricated from a high-purity titanium sheet (99.5%, Nilaco) sputtered with a pure transition-metal film for adjusting the chemical composition. All the ingots of the designed alloys were melted and inverted more than three times by plasma-arc melting in order to promote chemical homogeneity. They were rolled into 1-mm thick plates and then annealed in vacuum at 680 ºC for 2 h to remove residual strain. The transition metal concentration of the Ti-TM alloys was determined by inductively coupled plasma (ICP) analysis (CIROS 120 EOP, Rigaku). These results are shown in Table S1, indicating that the actual chemical composition of each designed alloy is close to its nominal composition.

Table S1 Transition metal content in Ti-TM alloys estimated by inductively coupled plasma (ICP) analysis

Sample	Contents（mass%）								
	Fe	Co	Ru	Cr	Cu	Mn	Ni	V	Zn
Ti-foil（Nilaco）	<0.01	<0.01	<0.01	<0.01	<0.01	<0.01	0.01	<0.01	<0.01
$Ti\text{-}Cr_{0.05}$ alloy	<0.01	<0.01	<0.01	0.06 (0.05at%)	0.01	<0.01	0.01	<0.01	<0.01
$Ti\text{-}V_{0.05}$ alloy	<0.01	<0.01	<0.01	0.01	<0.01	<0.01	0.01	0.05 (0.05at%)	<0.01
$Ti\text{-}Co_{0.06}$ alloy	<0.01	0.06 (0.06at%)	<0.01	0.01	<0.01	<0.01	0.01	<0.01	<0.01
$Ti\text{-}Fe_{0.05}$ alloy	0.06 (0.05at%)	<0.01	<0.01	0.01	0.01	<0.01	0.01	<0.01	<0.01
$Ti\text{-}Fe_{0.13}$ alloy	0.15 (0.13at%)	<0.01	<0.01	0.01	0.01	<0.01	0.01	<0.01	<0.01

Fabrication of Nitrogen and Transition-Metal Codoped TiO_2 Nanotube [(N,TM)-TNT]

Arrays: Ti-Low concentration TM (0.05–0.13 at%) alloys (Ti-TM alloys) were polished, cut into 3 cm×6 cm pieces, cleaned by sonicating in acetone and ethanol, rinsed with water and dried under an N_2 flux. The cleaned alloys were anodized at a constant potential of 40 V in an ethylene glycol solution containing 0.25 wt% NH_4F and 2 vol% H_2O for 1 h at room temperature in a two-electrode configuration with a platinum foil as the counter electrode. After anodization, the prepared samples were rinsed with water and dried at 80 ºC in air. The as-anodized samples were annealed in air at 500 ºC for 1 h. Finally, N-doping was carried out under NH_3/Ar flow at 575 ºC for 0.5 h.

Modification of Co-catalysts: The co-catalyst (Co-Bi) was electrochemically modified on nanotubes in solutions containing 0.1 mM $Co(NO_3)_2$ and 0.1 M Potassium borate aqueous solution using a standard three-electrode configuration comprising a TNT working electrode, a Pt counter electrode, and an Ag/AgCl reference electrode. Modification of Co-Bi on the TNTs was photoelectrodeposited at +0.6 V *vs.* Ag/AgCl under Xe-lamp irradiation until passage of 0.9 C.

FE-SEM observation of (N, TM)-TNTs

The morphology of the samples was characterized with a field-emission scanning electron microscope (FE-SEM; S5500, Hitachi).

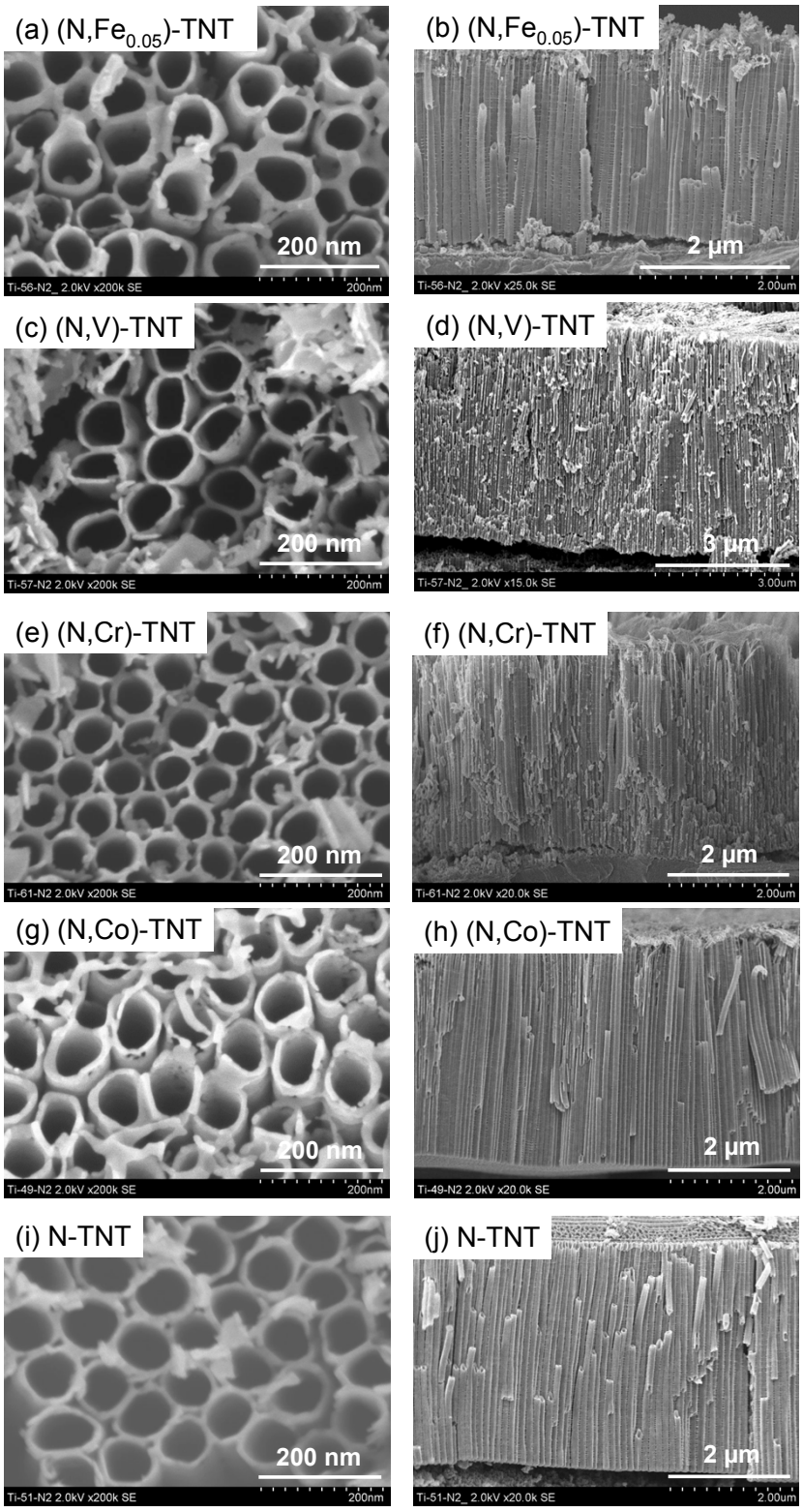

Fig. S1 (a)(c)(e)(g)(i) Top view and (b)(d)(f)(h)(j) cross-sectional view of FE-SEM images of various (N,TM)-TNTs and N-TNT.

XRD patterns of (N, TM)-TNTs

The crystal structure of the sample was measured with an X-ray diffractometer (RINT-TTR, Rigaku) using Cu Kα radiation at 50 kV and 300 mA.

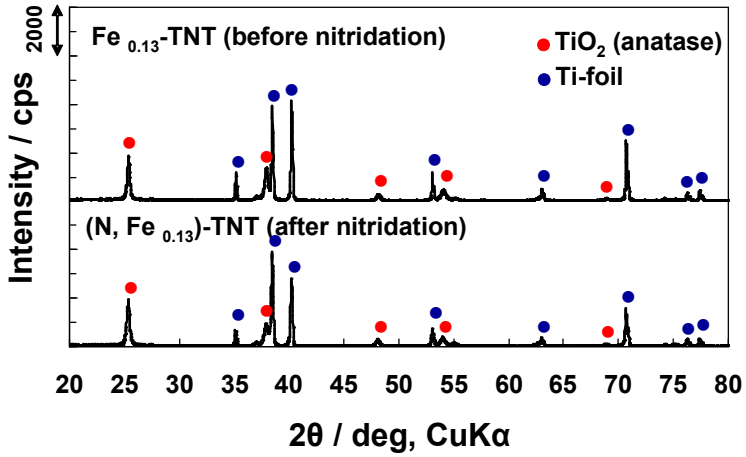

Fig. S2-1 XRD patterns of Fe $_{0.13}$-TNT crystallized at 500 ºC and (N, Fe $_{0.13}$)-TNT.

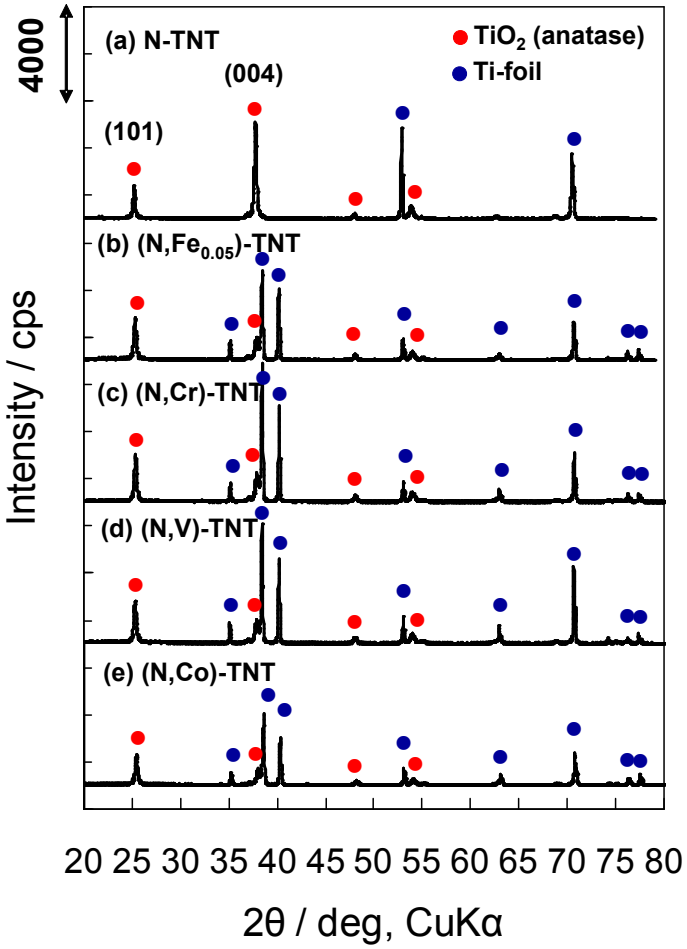

Fig. S2-2 XRD patterns of (N, TM)-TNTs and N-TNT.

XPS measurements of (N, TM)-TNT samples

The N states and N-doping concentrations in the samples were characterized with X-ray photoelectron spectroscopy (XPS; PHI-5500MC, ULVAC-PHI) using monochromated Al Kα radiation. Fig. S2 shows N 1*s* XPS spectra of various TNT samples. TNT and $Fe_{0.05}$-TNT without nitridation exhibit only one peak at 400 eV, while N-TNT and (N, Fe)-TNTs with nitridation showed an additional peak at 396 eV. Because this peak at 396 eV (N^{3-}) is assigned to be the substitutional N (β–N) at the O site in TiO_2 [1, 2], the results indicate that N-doping into TNTs was successfully achieved for obtaining high photocatalytic activity.

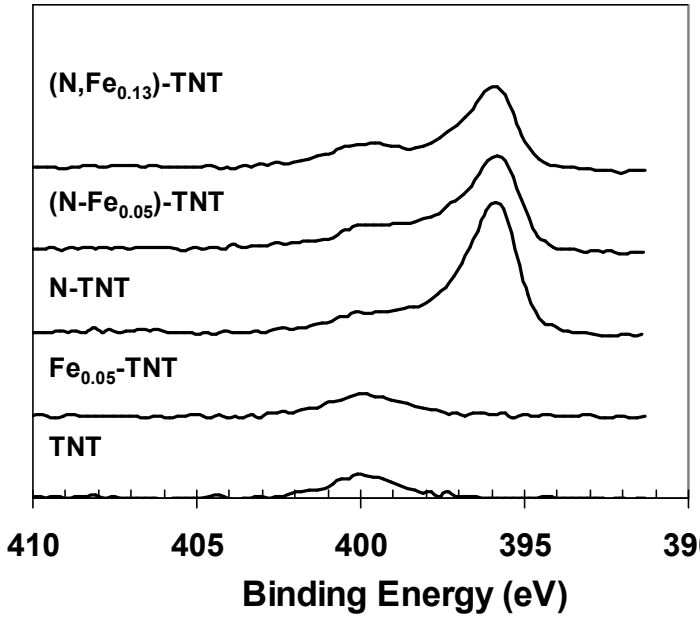

Fig. S3 XPS spectra of N 1s for the TNT, $Fe_{0.05}$-TNT, N-TNT, (N, $Fe_{0.05}$)-TNT, and (N, $Fe_{0.13}$)-TNT samples.

Table S2 N contents of (N, TM)-TNT samples

Sample	N content (at%)[a]
TNT	0.0
$Fe_{0.05}$-TNT	0.0
N-TNT	3.2
(N, $Fe_{0.05}$)-TNT	2.3
(N, $Fe_{0.13}$)-TNT	2.1
(N, Cr)-TNT	1.9
(N, V)-TNT	2.0
(N, Co)-TNT	2.2

[a] Estimated by XPS analysis.

Dynamic-SIMS(D-SIMS) of (N, TM)-TNTs:

D-SIMS depth profiling was performed with an ULVAC PHI SIMS6650 instrument. The primary ion was O_2^+ with an accelerating voltage of 5 kV, an ion current of 30 nA on average. The raster size for the analysis was 5% of the size used for the sputtering. The size of sputtering was 100×200 microns^2. As shown in Figure S4, it was identified that various TMs (Cr, V, and Co) which were doped in the nanotubes were well dispersed in the depth direction.

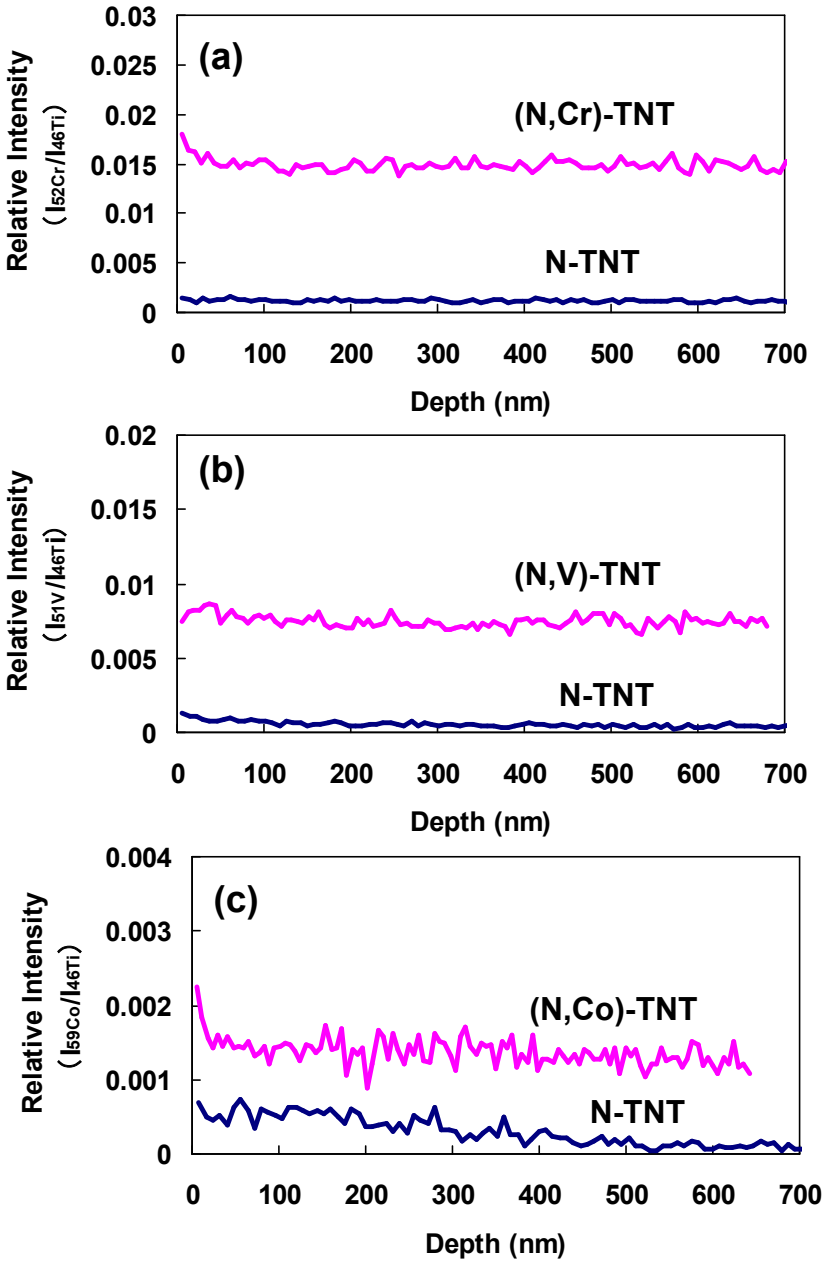

Fig. S4 D-SIMS depth profiling of (N, TM)-TNT samples.

TOF-SIMS of (N, TM)-TNTs:

TOF-SIMS measurements were performed with a TOF-SIMS V (ION-TOF GmbH, Münster, Germany) instrument using 30-keV Bi^+ primary ions in a high-current bunched mode. Positive spectra were acquired at five points, each with an area of 500×500 μm^2, for every sample. The total ion doses for these measurements were kept below 10^{12} ions/cm^2 to ensure a static SIMS condition. As shown in Fig. S5, various TMs (Fe, Cr, and Co) were detected.

Sputter depth profiling was performed in the dual-beam mode with 30-keV Bi^+ at a current of ~2 pA for analysis and 2-keV O_2^+ at a current of 500 nA for sputtering. The beam raster sizes were (150×150 μm^2) for the O_2 sputter beam and (50×50 μm^2) for the Bi analysis beam. The sputter depths were measured using a Dek-tak profilometer. As shown in Fig. S6, it was identified that Fe components which were doped in the nanotubes were dispersed in the depth direction.

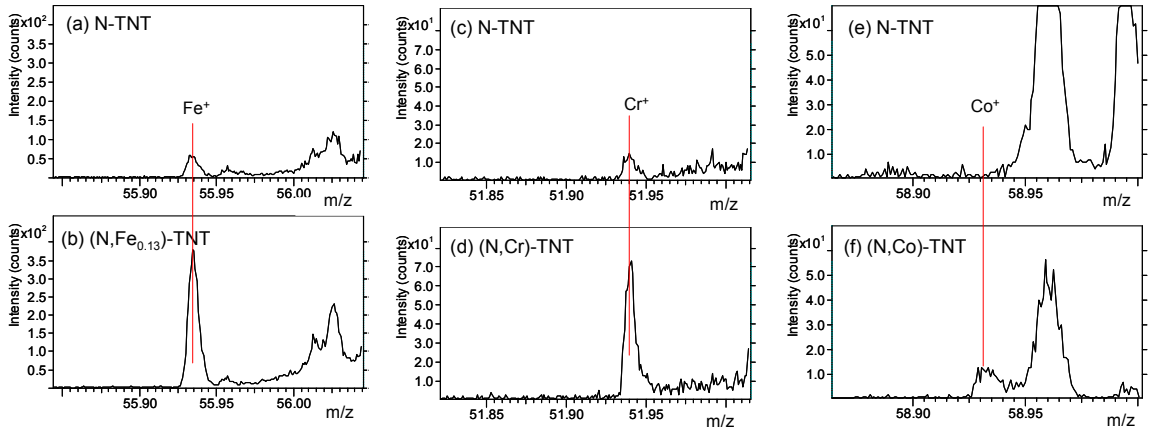

Fig. S5 TOF-SIMS positive spectra of the (N, TM)-TNT samples.

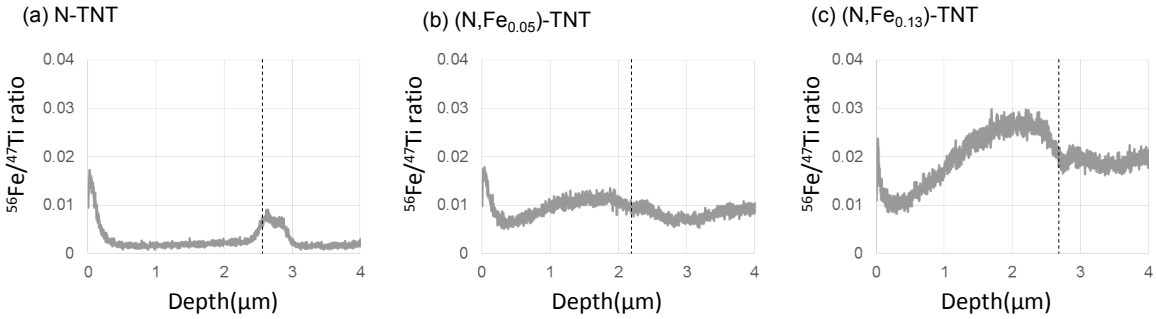

Fig. S6 Depth profiles showing $^{56}Fe/^{47}Ti$ ratios as a function of the sputter depth. Dotted lines are interfaces between TNTs and the Ti-foil as defined by the depth profiles of the $Na/^{47}Ti$ ratio.

Current-potential curves of TNT samples:

The photoelectrochemical behavior was investigated in 0.1 M KOH aqueous solution with a three-electrode configuration using an Ag/AgCl reference electrode and a Pt wire counter electrode. The experiments were purged with Ar gas and illuminated through a photoelectrochemical cell with visible light (300W Xe lamp <MAX-303, Asahi Spectra> with 42L filter, λ≥410 nm, 99.99%-cut-off).

Fig. S7-1 shows photocurrent-voltage curves for the TNT, $Fe_{0.13}$-TNT, N-TNT, (N, $Fe_{0.05}$)-TNT, and (N, $Fe_{0.13}$)-TNT samples measured under visible-light irradiation. Although N-doping in TNTs provides enhanced photocurrent under visible-light irradiation, Fe-doping was not effective for improving the visible photoresponse. It is worth noting that the codoping of both nitrogen and iron substantially improved the photocurrent of the TNT photoanode under visible-light irradiation. (N, $Fe_{0.13}$)-TNTs exhibited much higher photocurrent density than Fe $_{0.13}$-TNTs. The photocurrent of the N-Fe-TNT photoanode was also dependent on the amount of Fe. The photocurrent of (N-,Fe $_{0.13}$)-TNTs actually increased by 63% compared with (N, Fe $_{0.05}$)-TNTs (at +0.6 V vs Ag/AgCl). In addition, we have examined two different concentrations of Co dopants (0.06 and 0.15%) as shown in Fig. S7-2, in which we found that the photocurrent of (N, Co)-TNT was dependent on the amount and ratio of N and Co. The highest photo-oxidation current was observed for (N, Co-0.15%)-TNT at +0.6 V vs Ag/AgCl.

These results indicate that the amount of doping is one of the important factors in determining the photoelectrochemical properties.

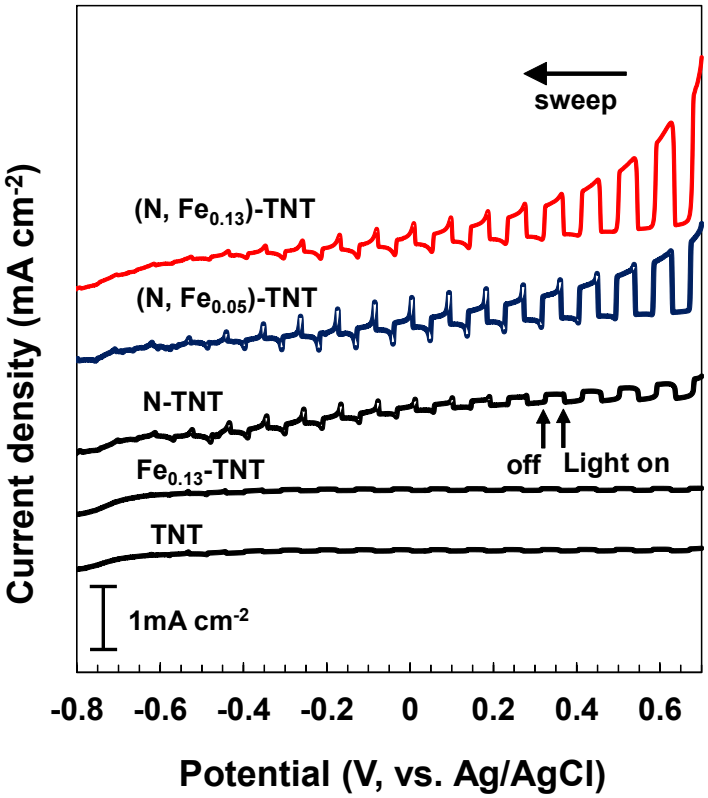

Fig. S7-1 Current-potential curves of the TNT, $Fe_{0.13}$-TNT, N-TNT, (N, $Fe_{0.05}$)-TNT, and (N, $Fe_{0.13}$)-TNT samples. The curves were measured in a 0.1 M aqueous KOH solution under chopped visible light (≥410 nm).

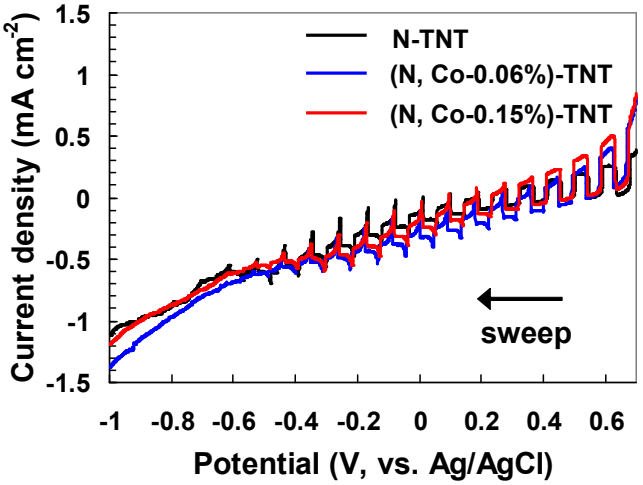

Fig. S7-2 Current-potential curves of N-TNT, (N, Co-0.06%)-TNT and (V, Co-0.15%)-TNT samples. The curves were measured in 0.1 M aqueous KOH solution under chopped visible light (≥410 nm).

Incident photon to charge carrier efficiency (IPCE) of TNT samples:

The photoelectrochemical behavior was investigated in 0.1 M KOH aqueous solution with a three-electrode configuration using an Ag/AgCl reference electrode and a Pt wire counter electrode at +0.6 V (vs Ag/AgCl). The wavelength dependence of IPCE [3] was measured under monochromatic irradiation from a Xe lamp equipped with bandpass filters (central wavelengths: 340, 360, 380, 400, 420, 440, 460, 480, 500, 520, 540, 560, 580, 600, 640, 680, 720, 760, and 800 nm).

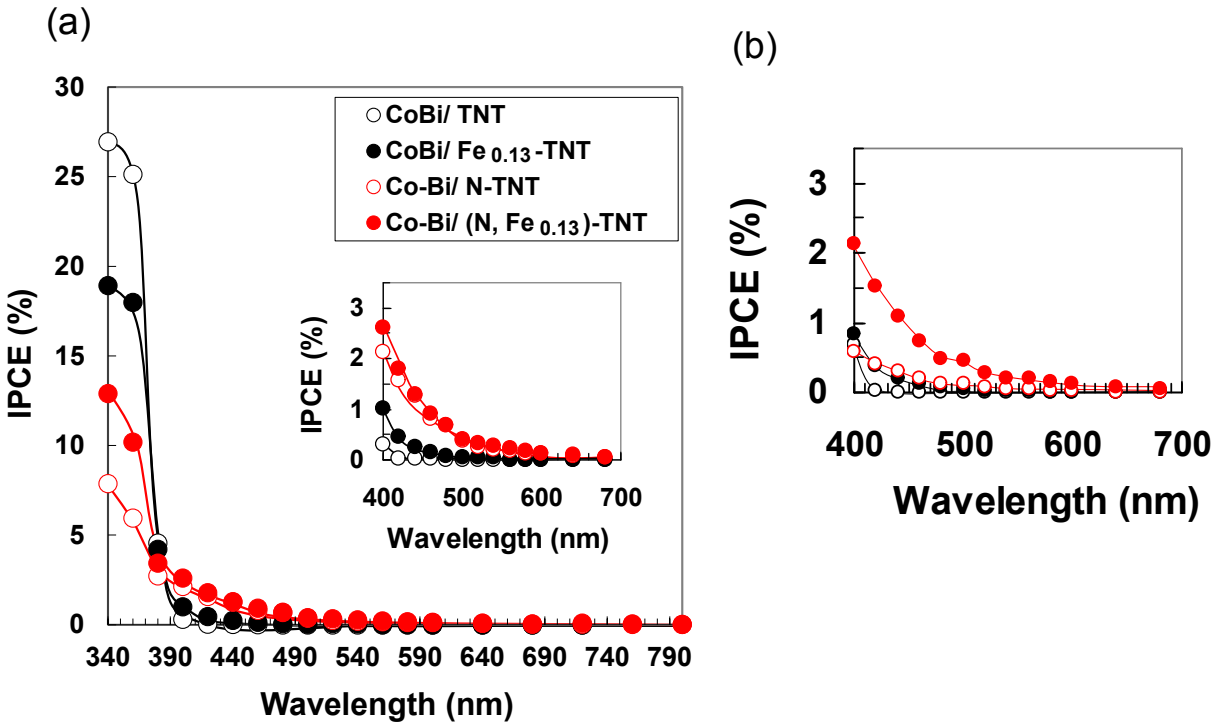

Fig. S8 (a) IPCE spectra of the TNT, $Fe_{0.13}$-TNT, N-TNT, and (N, $Fe_{0.13}$)-TNT which were loaded with Co-Bi. The spectra were collected at an incident wavelength range from 340 to 800 nm at a potential of +0.6 V (vs Ag/AgCl). Light intensity of Xe lamp was 31.7 mW/cm^2 (output power of 25 %) measured by a UV powermeter C9536-01 (Hamamatsu Photonics). (b) IPCE spectra in visible-light region measured with Xe lamp irradiation at 195 mW/cm^2 (output power of 100%, light intensity is equivalent to the condition of Fig. 3).

The amount of photogenerated O_2 over a Co-Bi/(N, $Fe_{0.13}$)-TNT photoanode was determined using an O_2 probe (NeoFOX, FOSPOR probe, Ocean Optics) [4]. Current-time measurements were conducted in the three-electrode configuration. A TNT photoanode, Ag/AgCl, and Pt wire electrode were used as the working, reference, and counter electrodes, respectively. 0.05 M $K_2B_4O_7$-0.2 M H_3BO_3 aqueous solution or 0.1 M KOH aqueous solution was used as the electrolyte and the applied potential was maintained at +0.6 V vs Ag/AgCl. First, the electrolyte was bubbled with Ar gas to remove O_2 within the system. Then, visible light (300 W Xe lamp <MAX-303, Asahi Spectra> with 42 L filter, $\lambda \geq 410$ nm) was irradiated onto the TNT photoanode for a predetermined time, and the photocurrent and O_2 concentration in the liquid phase or gas phase were measured.

The time profile of the amount of O_2 in the gas phase and the current observed over the Co-Bi/(N, $Fe_{0.13}$)-TNT photoanode are shown in Fig. S9. The data shows the amount of O_2 in the gas phase (at the headspace of the reactor, electrolyte: 0.1 M KOH) and the blue line indicates the theoretical amount of O_2 calculated by the observed photocurrent with 100% current efficiency. Although the amount of O_2 clearly increased upon light irradiation, the value was unstable because of the time lag in which O_2 moved from the electrolyte to the gas phase and was absorbed over the high surface area of the nanotube photoanode. However, the amount of O_2 almost corresponded to the theoretical amount. These results indicate that water splitting occurred in this reactor under visible-light irradiation.

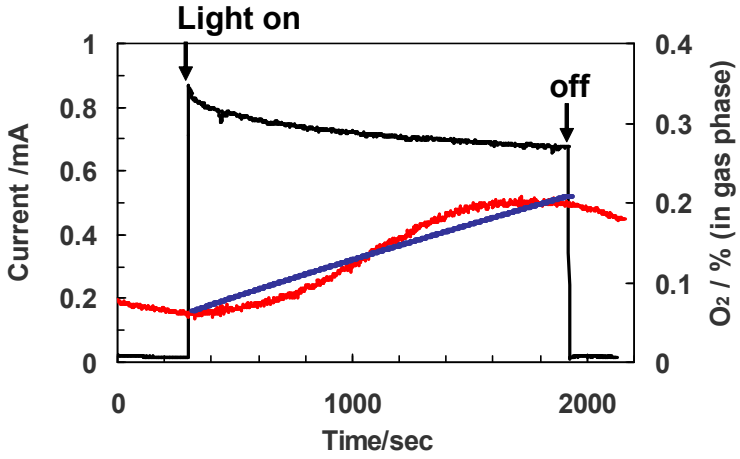

Fig. S9 Time profile of the current (black line, left vertical axis) and amount of O_2 (red line, right vertical axis) observed over the Co-Bi/(N, $Fe_{0.13}$)-TNT photoelectrode. O_2 was measured in the headspace of the cell (electrolyte: 0.1 M KOH, pH 12.8). The blue line indicates the theoretical amount of oxygen calculated by the observed photocurrent with 100% current efficiency.

Mott-Schottky analyses of TNT samples

The electrochemical impedance measurements TNT, $Fe_{0.13}$-TNT, N-TNT and (N, $Fe_{0.13}$)-TNT were carried out in the dark using a 3-electrode configuration. We also measured anatase TiO_2 film prepared by sputtering followede by postannealing at 500^{o}C as a reference. The electrode samples were scanned from 0.2 V to –1.0 V/ vs Ag/AgCl in 0.1 M KOH solution (pH 12.8) and the frequencies were varied from 0.5 kHz to 2 kHz for each potential. The amplitude of the AC signal was 10 mV. The Mott-Schottky analyses were performed according to ref 5 and the flatband potential of the semiconductor (E_{fb}) was calculated. Fig. S10-1 shows the Mott-Schottky plots of TNT samples and we confirmed almost the same flatband potential in all examined frequencies (0.5k, 1k and 2 kHz). Table S3 gives the results from the Mott-Schottky analyses, whose plots are presented in Fig. S10-2. Comparing with anatase TiO_2 film, the flatband potentials of TNTs are located at more positive position. The flatband potentials of TNTs shift negatively by doping of N or/and Fe doping, the order of the negative shift was found to be (N, Fe)>N>Fe>non-doping probably due to formation of O-vacancy induced by the unbalanced doping .

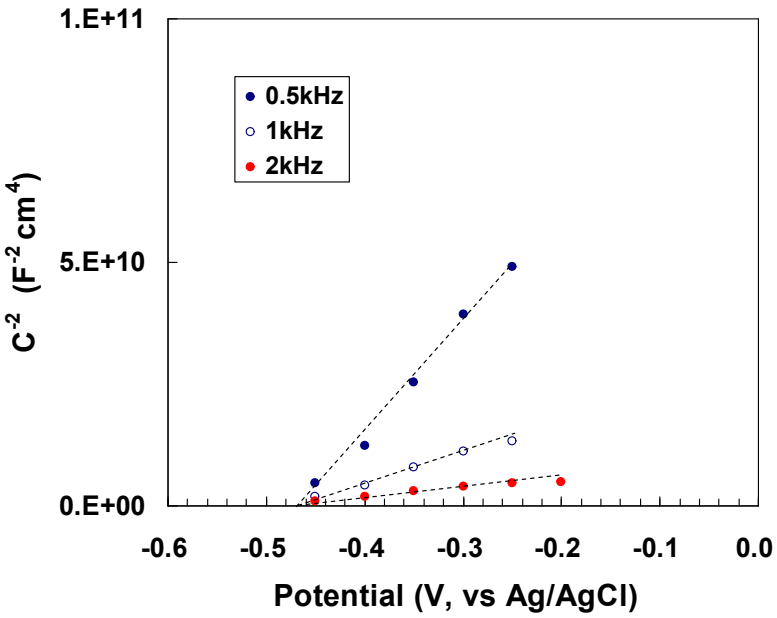

Fig. S10-1 Mott-Schottky plots for TNT measured in 0.1 M KOH solution (pH 12.8).

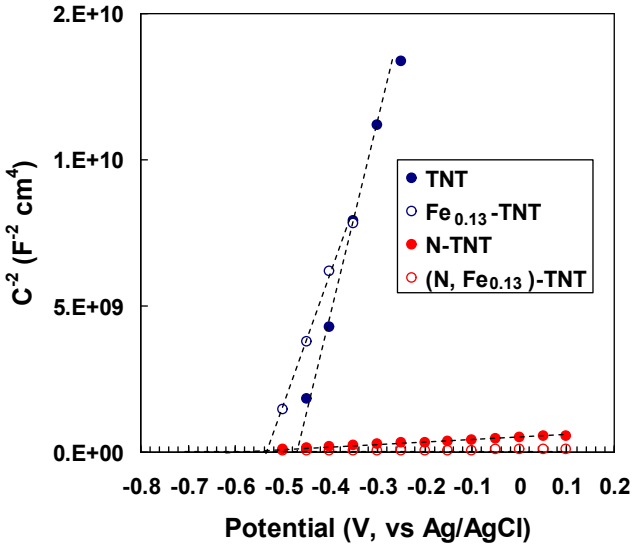

Fig. S10-2 Mott-Schottky plots for TNT, $Fe_{0.13}$-TNT, N-TNT and (N, $Fe_{0.13}$)-TNT measured in 0.1 M KOH solution (pH 12.8) at 1 kHz.

Table S3 Flatband potentials obtained from Mott-Schottky analysis of TNT samples and an anatase TiO_2 film.

Sample	E_{fb} (V, vs Ag/AgCl)
TNT	–0.47
Fe-TNT	–0.53
N-TNT	–0.64
(N, Fe)-TNT	–0.72
TiO_2 (sputtered)	–0.80

References

[1] R. Asahi, T. Morikawa, T. Ohwaki, K. Aoki and Y. Taga, *Science,* 2001, **293**, 269.

[2] R. Asahi, T. Morikawa, *Chem. Phys.,* 2007, **339**, 57.

[3] M. Higashi, K. Domen and R. Abe, *Energy Environ. Sci.,* 2011, **4**, 4138.

[4] D. K. Zhong, S. Choi and D. R. Gamelin, *J. Am. Chem. Soc.* 2011, **133**, 18370.

[5] A. Paracchino, N. Mathews, T. Hisatomi, M. Stefik, S. D. Tilley and M. Grätzel, *Energy Environ. Sci.,* 2012, **5**, 8673.